ACS APPLIED MATERIALS & INTERFACES

Research Article

www.acsami.org

Formation of Regular Stripes of Chemically Converted Graphene on Hydrophilic Substrates

Yufei Wang,[†] Yasushi Mino,[‡] Satoshi Watanabe,*[,‡] Dan Li,[†] and Xuehua Zhang*[,§]

[†]Department of Materials Engineering, Monash University, VIC, 3800, Australia

[‡]Department of Chemical Engineering, Kyoto University, Katsura, Nishikyo, Kyoto, 615-8510, Japan

[§]Department of Chemical and Biomolecular Engineering and Particulate Fluid Processing Center, University of Melbourne, Parkville, 3010, Australia

Supporting Information

ABSTRACT: Chemically converted graphene (CCG), from a chemistry point of view, is a giant molecule with a unique two-dimensional (2D) configuration. The availability of CCG dispersion provides a range of scalable methods to assemble graphene-based materials but brings the challenge of understanding and control of the CCG morphology in solution processing. In this study, we found that, similar to conventional colloidal systems (e.g., spherical particles or polymers), a 2D sheet of CCG can be transferred from its aqueous dispersion to solid substrates in the form of highly regular stripe patterns by evaporation-driven deposition. The width and spacing can be defined by the concentration of the CCG dispersion and the properties of the substrate (e.g., roughness and surface charge). Furthermore, the high resolution AFM images illustrate that both 2D flattened and highly wrinkled CCG can be formed in each individual stripe, depending on the location across the stripe. The in situ optical observation of the stripe formation indicates that the morphological change of CCG may occur in the crowded meniscus of the drying front.

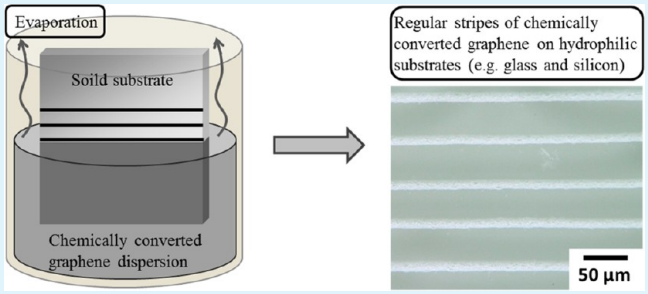

KEYWORDS: *chemically converted graphene, self-assembly, regular stripe pattern, hydrophilic surfaces*

INTRODUCTION

Graphene, owing to its extraordinary electronic, mechanical, and thermal properties,[1,2] has received substantial attention from various fields, such as electronics,[3,4] photonics,[5,6] and energy storage.[6−9] Among the numerous fabrication methods, the preparation of chemically converted graphene (CCG) provides a facile and cost-effective approach to obtaining graphene sheets.[10] In particular, the aqueous dispersion of CCG contains a large amount of individually separated 2D sheets.[11,12] One of the major challenges is the controlled and reproducible transfer of CCG from the dispersion to a stable and structured dry state, because the single-atomic CCG sheets are intrinsically flexible and susceptible to the external conditions during the processing.[6,13]

A great deal of effort has been made to achieve controlled assembly of structured graphene patterns, such as lithographic techniques, chemical vapor deposition, and inkjet printing.[14−20] Huang and co-workers found that the regulation of the morphology of GO sheets has a significant impact on its electrical and optical properties.[21] Evaporation-driven assembly is one of the most effective approaches for the fabrication of functional structures from nanoscale building blocks,[22−25] and it has been successfully used in the assembly of colloidal nanoparticles, block copolymers, and carbon nanotubes.[15,16,18,20,22−31] However, it remains largely unknown about how to assemble the 2D CCG into regular patterns. Only recently, Yang and co-workers reported the fabrication of self-organized graphene patterns by solvent evaporation using poly(ionic liquid) modified graphene,[28] casting a light on engineering low-cost graphene-based functional materials with a simple fabrication process.

Our attention is paid to the effect of the drying process on the morphology of deposited CCG sheets on solid surfaces without the presence of additives. We have previously found that the drying process can induce the flattening and self-assembly of monolayer CCG on negatively charged hydrophilic solid substrates.[29,32] Other groups have also revealed the similar self-assembly behavior of either CCG or graphene oxide (GO) by drying.[28,33−37] To the best of our knowledge, there is no report about the effect of drying on the morphology of multilayer CCG sheets and their properties. In this work, we show that regular CCG stripe patterns can be produced over a large surface area by convective deposition techniques. The width of CCG stripes and the spacing between neighboring stripes can be rationally tuned by careful control of the experimental conditions. Furthermore, we observed in situ the

Received: March 28, 2013
Accepted: May 31, 2013
Published: May 31, 2013

formation process of the CCG stripe pattern and found the location-dependent morphology of both monolayer and multilayer CCG.

EXPERIMENTAL SECTION

1. Preparation of CCG Dispersion and Substrates. The CCG solution was prepared by chemical reduction of a graphene oxide (GO) solution, and the details have been reported in our previous publication.[10] The solvent is water with less than 0.35% ammonia, which ensures stability of the CCG sheets in water. The concentration of the CCG dispersion can be easily tuned by dilution, and the concentration used in this work ranges from 0.001 mg/mL to 0.01 mg/mL.

The silicon and glass substrates were cleaned by piranha solutions at 75 °C for 30 min, followed by rinsing with Milli-Q water and drying with nitrogen of high purity. The mica was freshly cleaved before use. The poly(diallyldimethylammonium chloride) coated mica (PDMA-mica) surfaces were prepared by immersing the freshly cleaved mica in 1 wt % PDMA solution for 30 min, followed by rinsing with Milli-Q water and drying with a nitrogen stream.

2. Fabrication of CCG Patterns. To fabricate the regular CCG stripe pattern, the substrates were vertically immersed into a CCG aqueous dispersion with a certain concentration. In this work, 20 mL of slightly preheated CCG dispersion was used for stripe fabrication, and the diameter of the glass vessel containing CCG dispersion is approximately 3 cm. The whole setup was then left in an oven at 60 °C overnight, and the stripe patterns were formed during solvent evaporation.

3. Characterizations. The stripe patterns can be directly observed from the optical microscope, and the formation process was captured by a camera (BX51, OLYMPUS, Japan). The morphology of the CCG stripe pattern was characterized by atomic force microscopy (Mulitmode IV, Bruker). The samples were imaged with the tapping mode in the air using the cantilever with a spring constant of 40 N/m (Budget Sensors Tap-300G-Al). Raman spectra were obtained from an an Ar laser (Renishaw Invia) with an excitation line at 514.5 nm. X-ray photoelectron spectroscopy (XPS) was carried out using a VG ESCALAB220i-XL spectrometer equipped with a hemispherical analyzer.

RESULTS AND DISCUSSIONS

1. Effects of the CCG Concentration. As shown in Figure 1, a hydrophilic substrate was vertically immersed into CCG dispersion, and regular CCG stripe patterns can be formed during solvent evaporation. Raman and X-ray photoelectron spectroscopy (XPS) analyses were performed to characterize the chemical structure of CCG stripes on glass. Two prominent bands at 1348 and 1583 cm^{-1} are clearly shown in the Raman spectrum of CCG stripes on glass, and they represent the D and G bands of carbon, respectively (Figure S1a).[38] Moreover, the presence of four types of carbon bonds—C−C/C═C bond at 285.0 eV, C−O bond at 286.2 eV, C═O bond at 287.3 eV, and O−C═O at 288.5 eV—was illustrated from the C 1s XPS spectrum of CCG stripes on a glass substrate (Figure S1b).

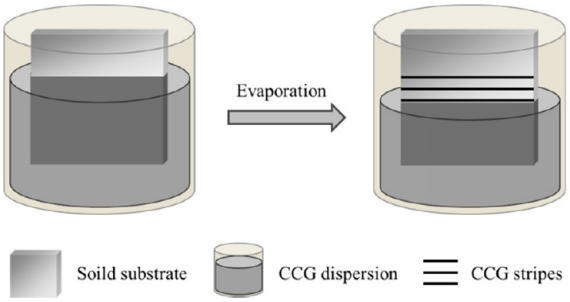

Figure 1. Schematic diagram of the formation of CCG stripes on hydrophilic surfaces by convective deposition techniques during solvent evaporation.

In the first set of experiments, we studied the effect of CCG concentration on the stripe formation on hydrophilic glass. We could not obtain the CCG stripe patterns when the CCG concentration was higher than 0.05 mg/mL (Figure S2a). When the CCG concentration was reduced to 0.01 mg/mL, regular stripe patterns were produced and clearly visible under optical microscopy. Figure 2a−e show the optical images of the patterns on a hydrophilic glass substrate, and more images are provided in Figure S3. The stripes are straight and aligned in parallel with the neighboring stripes. They extend as long as the substrate is (i.e., 2 cm here) and distribute over the entire substrate.

The average width of the stripes and the spacing between neighboring stripes were measured from the optical images, and they are found to be dependent on the concentration of CCG dispersion (Figure 2f−g). As the concentration of CCG dispersion increases from 0.001 mg/mL to 0.01 mg/mL, the width of the stripe gradually increases from 6.7 ± 1.0 μm to 9.6 ± 1.1 μm, and the spacing between two stripes is also slightly increased from 20.7 ± 4.2 μm to 26.1 ± 4.0 μm.

The morphology of the individual stripe was further characterized by atomic force microscopy (AFM). Figure 3a,b show the AFM image of an individual CCG stripe prepared from 0.001 mg/mL of CCG suspension and the representative cross-sectional profile. Clearly the height of the stripe is not uniform. From the "top" where the stripe starts forming to the "bottom" where the stripe ends, the height of the stripe gradually increases (Figure 3b), followed by a sharp decrease. Interestingly, the height of the stripe is approximately 37 nm for all samples prepared from CCG dispersions with concentrations from 0.001 mg/mL to 0.01 mg/mL (Figure 3c). The concentration of the CCG dispersion has little influence on the height of the CCG stripe, in contrast to its significant impact on the stripe width and spacing. In addition, the spacing between CCG stripes is also characterized, showing a limited amount of randomly distributed CCG sheets (Figure S4).

2. Effects of the Roughness and Charges of the Substrate. In this section, we studied the effect of the surface roughness and surface charges on the formation of CCG stripe patterns. First we compared two hydrophilic surfaces, glass and silicon. The roughness of the glass slide is measured to be about 1.4 nm, and that of the silicon surface is about 0.1 nm. Regular stripe patterns were successfully produced on the hydrophilic silicon substrate (Figure 4a−d), similar to the above results on the hydrophilic glass substrate. The AFM image is shown in Figure 4e, and the height profile of the stripe presents similar features to those on a glass surface—the CCG stripe grows with the liquid level going down, followed by a sharp ending (Figure 4f).

The measurement of stripe width and the spacing between stripes also obtains concentration-dependent results as shown in Figure 4g,h. With the increase of the CCG concentration from 0.001 mg/mL to 0.0075 mg/mL, interestingly the width of the stripe has significantly decreased from 30.0 ± 3.9 μm to 11.4 ± 1.9 μm while the spacing between two stripes ha slargely reduced from 53.0 ± 6.1 μm to 30.6 ± 3.4 μm, respectively. So the stripes become thinner but denser with the increase of the

dx.doi.org/10.1021/am401918f | ACS Appl. Mater. Interfaces 2013, 5, 6176−6181

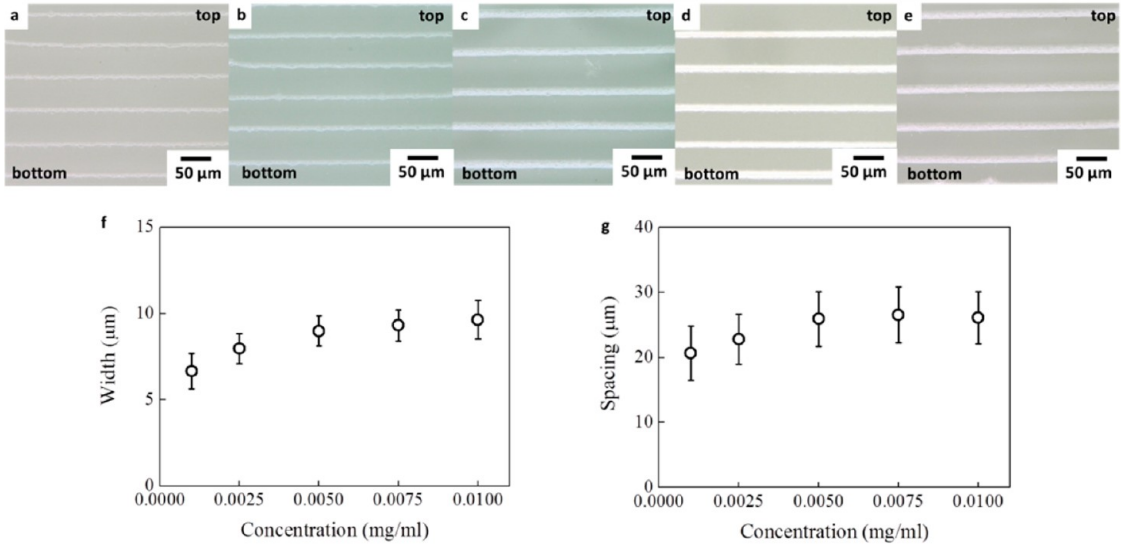

Figure 2. Optical microscopic images of CCG stripes on a glass substrate formed by CCG dispersions with concentrations of (a) 0.001 mg/mL, (b) 0.0025 mg/mL, (c) 0.005 mg/mL, (d) 0.0075 mg/mL, and (e) 0.01 mg/mL in the oven at 60 °C and the effect of concentration of CCG dispersion on (f) the width of CCG stripes and (g) the spacing between neighboring CCG stripes. Note that the average width and spacing are measured from the optical microscopic images.

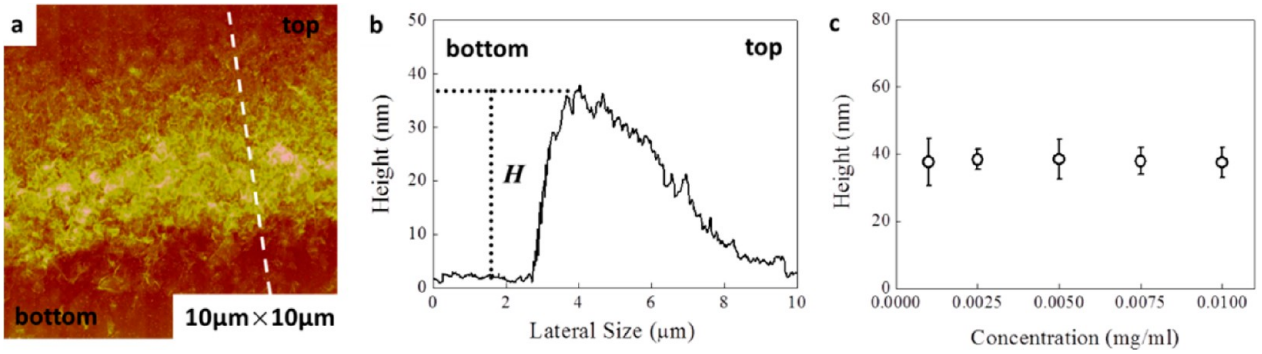

Figure 3. (a) AFM image of one CCG stripe on a glass substrate prepared with a CCG concentration of 0.001 mg/mL. (b) The height profile of the dashed line in a. The height of the stripe (H) is measured from the top of the stripe to the surface. (c) the effect of the concentration of CCG dispersion on the height of the CCG stripes. Note that the average height of the stripe is measured by taking the average distance between the stripe and the surface at the point where the stripe formation finishes.

CCG concentration, which is somehow different from the trends on a glass substrate. In addition, if the CCG dispersion with a concentration of 0.01 mg/mL was used, a nonuniform film is formed on the silicon substrate, rather than stripe patterns (Figure S2b).

When the surface charge was varied, completely different results were obtained. In this work, two types of substrates were studied: negatively charged hydrophilic surfaces (e.g., glass, silicon, and mica) and a positively charged surface (e.g., poly(diallyldimethylammonium chloride) modified mica (PDMA-mica)). The stripe patterns on the mica surface were similar to those on glass or silicon (Figure S5). However, there is no stripe pattern observed on the PDMA-mica surface (Figure S6). This indicates that the electrostatic interactions between negatively charged CCG sheets and the positively charged PDMA-mica surface may hinder the formation of stripe patterns.

3. Morphology of CCG Stripes. Interestingly, we found that the morphology of CCG varies at different locations across a stripe. As shown in Figure 5a–d, the flat or slightly corrugated 2D CCG was mainly deposited at the top of the CCG stripe, or scarcely distributed in the space between the neighboring stripes, while the highly wrinkled CCG was at the middle and the bottom of the stripe. More AFM images are provided in Figures S7–S11 and show similar results.

For comparison, graphene oxide (GO) was deposited on the substrate following the same protocol, and regular GO stripes can be obtained in a similar manner. But across an individual stripe, all the GO sheets are stacked in a face-to-face manner without obvious corrugation (Figure 5e–g).

4. Properties of CCG Stripes. The directional structure from the stripes can render some anisotropic properties to the substrate. For example, the electrical property of the stripe patterns was measured by using the two-probe method with the use of thin gold film contacts. The gold electrode crosses over 46 CCG stripes, and the distance between the electrodes is 5 mm. As a result, the resistance of the CCG stripe is measured to be 246 kΩ along the stripe direction, and the corresponding resistivity is calculated to be 2.4×10^{-3} Ωm. However, the resistance in the direction vertical to the stripes is not measurable. On the other hand, the deposition of CCG stripes on hydrophilic surfaces can also affect the transparency. With

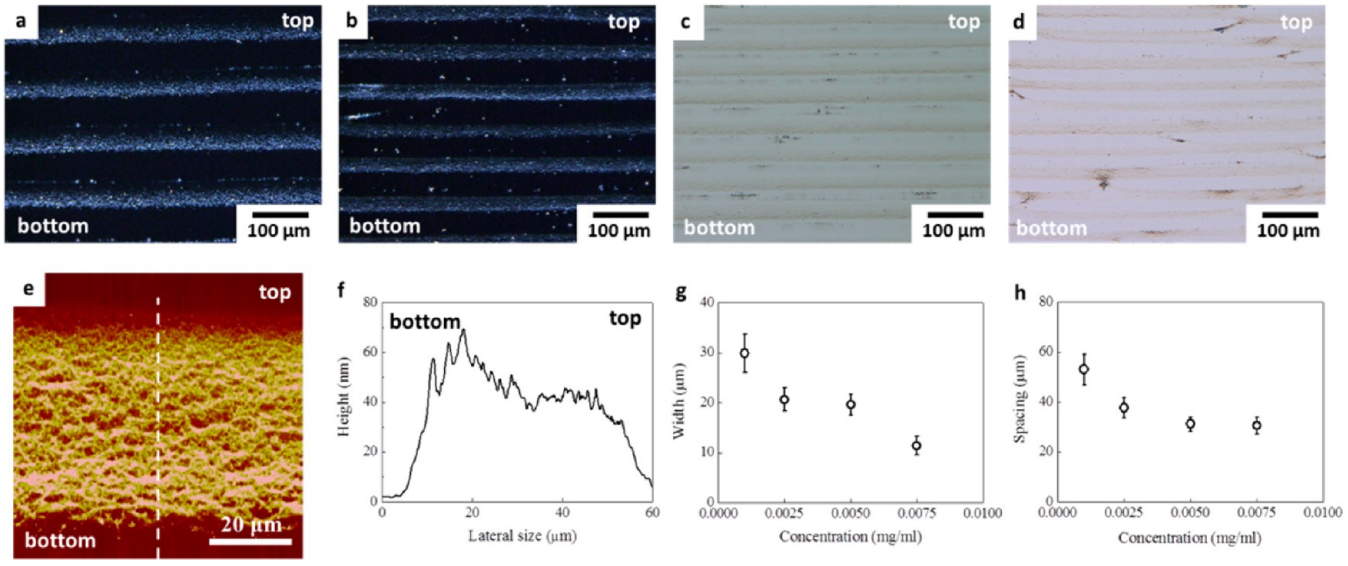

Figure 4. Optical microscopic images of CCG stripes on a silicon substrate formed by CCG dispersions with concentrations of (a) 0.001 mg/mL, (b) 0.0025 mg/mL, (c) 0.005 mg/mL, and (d) 0.0075 mg/mL in the oven at 60 °C. (e) AFM image of one CCG stripe in a and (f) height profile of the dashed line in e and the effect of concentration of CCG dispersion on (g) the width of CCG stripes and (h) the spacing between neighboring CCG stripes.

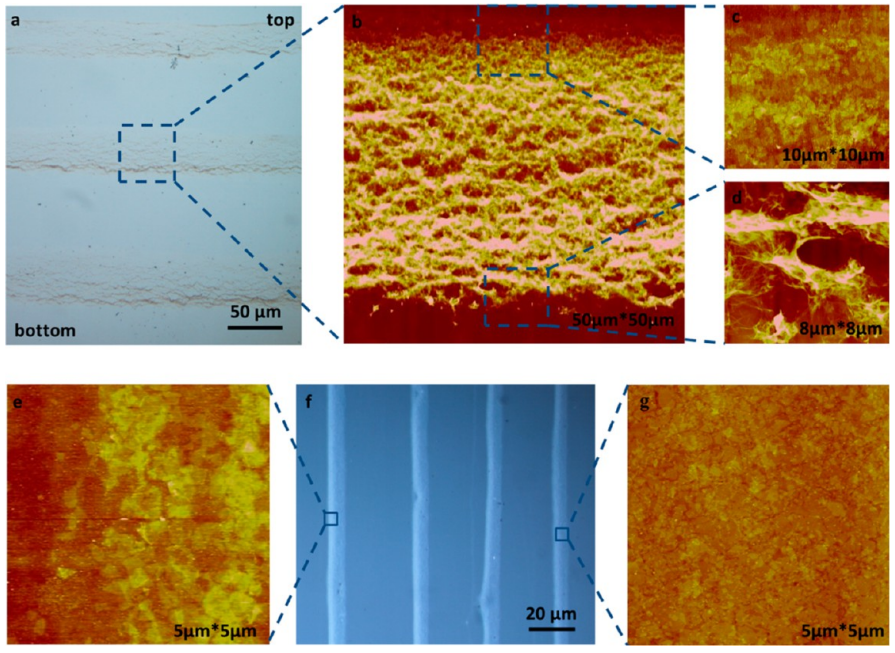

Figure 5. AFM images of (a) CCG stripe on silicon substrate and (f) GO stripe on glass substrate prepared by CCG or GO dispersion with a concentration of 0.005 mg/mL in the oven at 60 °C and the AFM images of the details in (b–d) CCG and (e, g) GO stripe.

the use of air for background adjustment, the transmittance of the CCG stripe pattern treated glass surfaces is found to be nearly 80% in the visible range for all of the samples prepared by CCG dispersion with different concentrations (Figure S12).

5. Dynamics of the Stripe Formation. To understand the mechanism governing the morphology of CCG stripes, we monitored the deposition process by optical microscopy. The snapshots are shown in Figure 6, and the video is provided in the Supporting Information. In Figure 6a, the contact line of the liquid is first pinned on the surface as indicated by the dark line in the images. The deposited area then becomes darker, indicating that more and more CCG sheets are transported from the dispersion to the drying front (Figure 6b). Note that the width of this deposited area is constant with time. In Figure 6c, the diffusive region at the bottom of the strip is clearly visible. While the region of the stripe becomes even more crowded, some wavy patterns gradually appear along the stripes, resembling honey flowing down a wall.[38]

The interference fringes then appear under the stripes as the liquid film thinned with the evaporation. Eventually the thin liquid film ruptures, and a hole is formed on the left-hand side (Figure 6d). The hole extends quickly from the left to the right, and the liquid film breaks off from the stripe (Figure 6e). Finally, the stripe becomes dried, and the receded liquid film is pinned in a new position where another CCG stripe starts to form following the same pinning–depinning process (Figure

dx.doi.org/10.1021/am401918f | ACS Appl. Mater. Interfaces 2013, 5, 6176–6181

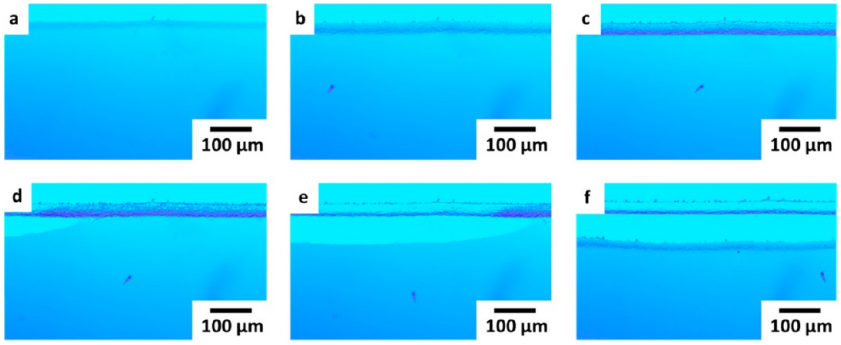

Figure 6. Snapshots of the formation of CCG stripe. (a) The liquid level gradually goes down. (b) A hole forms, and the CCG stripe starts to form. (c) The hole expands to break the liquid film. (d) The CCG stripe is formed, and the liquid level is entirely retracted to start forming a new CCG stripe.

6f). The formation process of the CCG stripes is quite similar to that of colloidal particles reported by Watanabe et al.,[15] where the receding of the liquid is dominated by the stability limit of the thin liquid film, not the stick−slip motion of the drying front.[23]

We suggest the following process for stripe formation. CCG sheets are originally in the form of corrugated 2D sheets in the dispersion[13] and are transported to the drying front by the convective flow to the tip of the meniscus induced by the evaporation. The wedge of the liquid front provides the limitation for the transport of CCG from the bulk dispersion. Due to the high wettability of the substrate, the liquid film can spread very thin on the substrate, so at the upper boundary of the stripes, only single layer sheets are deposited on the substrate and are flattened and self-assembled to an edge-to-edge configuration. This scenario is similar to what we observed on hydrophilic negatively charge substrates in a previous work.[29] With the increase of the liquid film thickness to the upper region of the stretched meniscus, a limited amount of CCG can be transported and deposited there, and hence the thickness of the stripes goes up. Most of the CCG sheets are jammed at the middle and lower regions of the meniscus. Due to such a "traffic jam," the local concentration of CCG increases. It is possible that before drying, the enhanced interactions between sheets in the crowded dispersion have already led to the crumpling of the stripes. The wavy features of the stripes may be due to the high viscosity of the dispersion before drying. The whole stripes become suddenly dry when the liquid ruptures due to the instability of the thinning. The apparently trivial difference in the roughness of silicon and glass might have influenced the strength of the pinning and the shape of the meniscus before the instability; therefore the CCG concentration has influenced the spacing and the width of stripes on them in different ways.

In this way, we may explain that since the height of the stripe is mainly dependent on the shape of the meniscus, the CCG concentration has little impact on the height of the stripes. In comparison to GO, since GO sheets possess a large amount of negatively charged oxygen-containing functional groups, we suggest that these functional groups may prevent the GO sheets from wrinkling in the traffic jamming. So a face-to-face deposition is obtained from GO dispersion.

CONCLUSION

In conclusion, regular CCG stripe patterns can be formed on negatively charged hydrophilic surfaces by using a convective deposition technique. The stripe width and the spacing between neighboring stripes are highly dependent on the concentration of the CCG dispersion and the nature of the substrates. Surprisingly, the morphology of CCG varies at different locations along the individual stripe. The flat CCG sheets were mainly distributed at the top of the stripe or in the space between stripes, while their highly wrinkled forms were found at the bottom. The in situ observation of the stripe formation shows that the highly crumpled structures in the middle and lower regions of the stripes may be due to the crowding effect in the drying front.

ASSOCIATED CONTENT

Supporting Information

Excited Raman spectra and XPS characterization, photos of the formation of non-uniform CCG film on the glass and silicon substrates, optical microscopic images, AFM images, and an optical transmittance plot. A video is also available. This material is available free of charge via the Internet at http://pubs.acs.org.

AUTHOR INFORMATION

Corresponding Author

*E-mail: nabe@cheme.kyoto-u.ac.jp, xuehuaz@unimelb.edu.au.

Author Contributions

The manuscript was written through contributions of all authors. All authors have given approval to the final version of the manuscript.

Notes

The authors declare no competing financial interest.

ACKNOWLEDGMENTS

This research was supported under Australian Research Council. X.H.Z. and D.L. are ARC Future Fellows.

REFERENCES

(1) Novoselov, K. S.; Geim, A. K.; Morozov, S. V.; Jiang, D.; Zhang, Y.; Dubonos, S. V.; Grigorieva, I. V.; Firsov, A. A. *Science* **2004**, *306*, 666−669.

(2) Allen, M. J.; Tung, V. C.; Kaner, R. B. *Chem. Rev.* **2010**, *110*, 132−145.

(3) Brey, L.; Fertig, H. A. *Phys. Rev. B* **2006**, *73*, 235411/1−235411/5.

(4) Son, Y. W.; Cohen, M. L.; Louie, S. G. *Phys. Rev. Lett.* **2006**, *97*, 216803.

(5) Bonaccorso, F.; Sun, Z.; Hasan, T.; Ferrari, A. C. *Nat. Photonics* **2010**, *4*, 611−622.

(6) Bao, Q. L.; Loh, K. P. *ACS Nano* **2012**, *6*, 3677−3694.

(7) Vivekchand, S. R. C.; Rout, C. S.; Subrahmanyam, K. S.; Govindaraj, A.; Rao, C. N. R. *J. Chem. Sci.* **2008**, *120*, 9−13.
(8) Wang, X.; Zhi, L. J.; Mullen, K. *Nano Lett.* **2008**, *8*, 323−327.
(9) Yoo, E.; Kim, J.; Hosono, E.; Zhou, H.; Kudo, T.; Honma, I. *Nano Lett.* **2008**, *8*, 2277−2282.
(10) Li, D.; Muller, M. B.; Gilje, S.; Kaner, R. B.; Wallace, G. G. *Nat. Nanotechnol.* **2008**, *3*, 101−105.
(11) Li, D.; Kaner, R. B. *Science* **2008**, *320*, 1170−1171.
(12) Xu, Y. X.; Shi, G. Q. *J. Mater. Chem.* **2011**, *21*, 3311−3323.
(13) Qiu, L.; Zhang, X. H.; Yang, W. R.; Wang, Y. F.; Simon, G. P.; Li, D. *Chem. Commun.* **2011**, *47*, 5810−5812.
(14) Pang, S. P.; Tsao, H. N.; Feng, X. L.; Mullen, K. *Adv. Mater.* **2009**, *21*, 3488−3491.
(15) Watanabe, S.; Inukai, K.; Mizuta, S.; Miyahara, M. T. *Langmuir* **2009**, *25*, 7287−7295.
(16) Lee, S. W.; Park, S. C.; Lim, Y.; Lee, B.; Leek, S. D. *Adv. Mater.* **2010**, *22*, 4172−4175.
(17) Torrisi, F.; Hasan, T.; Wu, W. P.; Sun, Z. P.; Lombardo, A.; Kulmala, T. S.; Hsieh, G. W.; Jung, S. J.; Bonaccorso, F.; Paul, P. J.; Chu, D. P.; Ferrari, A. C. *ACS Nano* **2012**, *6*, 2992−3006.
(18) Byun, M.; Bowden, N. B.; Lin, Z. Q. *Nano Lett.* **2010**, *10*, 3111−3117.
(19) Liu, W.; Jackson, B. L.; Zhu, J.; Miao, C. Q.; Chung, C. H.; Park, Y. J.; Sun, K.; Woo, J.; Xie, Y. H. *ACS Nano* **2010**, *4*, 3927−3932.
(20) Hong, S. W.; Jeong, W.; Ko, H.; Kessler, M. R.; Tsukruk, V. V.; Lin, Z. Q. *Adv. Funct. Mater.* **2008**, *18*, 2114−2122.
(21) Cote, L. J.; Kim, J.; Zhang, Z.; Sun, C.; Huang, J. X. *Soft Matter* **2010**, *6*, 6096−6101.
(22) Duggal, R.; Hussain, F.; Pasquali, M. *Adv. Mater.* **2006**, *18*, 29−34.
(23) Thompson, P. A.; Robbins, M. O. *Science* **1990**, *250*, 792−794.
(24) Lin, Z. *Evaporative Self-Assembly of Ordered Complex Structures*; World Scientific: River Edge, NJ, 2012.
(25) Sinitskii, A.; Tour, J. M. *J. Am. Chem. Soc.* **2010**, *132*, 14730−14732.
(26) Mino, Y.; Watanabe, S.; Miyahara, M. T. *Langmuir* **2011**, *27*, 5290−5295.
(27) Hong, S. W.; Byun, M.; Lin, Z. Q. *Angew. Chem., Int. Ed.* **2009**, *48*, 512−516.
(28) Kim, T. Y.; Kwon, S. W.; Park, S. J.; Yoon, D. H.; Suh, K. S.; Yang, W. S. *Adv. Mater.* **2011**, *23*, 2734−2738.
(29) Wang, Y.; Song, Y.; Watanabe, S.; Zhang, S.; Li, D.; Zhang, X. *ACS Appl. Mater. Interfaces* **2012**, *4*, 6443−6449.
(30) Huang, J.; Kim, F.; Tao, A. R.; Connor, S.; Yang, P. *Nat. Mater.* **2005**, *4*, 896−900.
(31) Cheng, C.; Li, D. *Adv. Mater.* **2013**, *25*, 13−30.
(32) Wadhwa, R.; Lagenaur, C. F.; Cui, X. T. *J. Controlled Release* **2006**, *110*, 531−541.
(33) Cote, L. J.; Kim, F.; Huang, J. X. *J. Am. Chem. Soc.* **2009**, *131*, 1043−1049.
(34) Cote, L. J.; Kim, J.; Tung, V. C.; Luo, J. Y.; Kim, F.; Huang, J. X. *Pure Appl. Chem.* **2011**, *83*, 95−110.
(35) Kim, J.; Cote, L. J.; Kim, F.; Yuan, W.; Shull, K. R.; Huang, J. X. *J. Am. Chem. Soc.* **2010**, *132*, 8180−8186.
(36) Xu, Y. X.; Sheng, K. X.; Li, C.; Shi, G. Q. *ACS Nano* **2010**, *4*, 4324−4330.
(37) Bai, H.; Li, C.; Wang, X. L.; Shi, G. Q. *J. Phys. Chem. C* **2011**, *115*, 5545−5551.
(38) Kudin, K. N.; Ozbas, B.; Schniepp, H. C.; Prud'homme, R. K.; Aksay, I. A.; Car, R. *Nano Lett.* **2007**, *8*, 36−41.